

Study of Energy Spectra and Electromagnetic moments of Double Beta Decay Nuclei in Deformed Hartree-Fock Model

S. K. Ghorui^{1,*}, P. K. Raina^{1,2}, A. K. Singh¹, P. K. Rath³, C. R. Praharaj⁴

¹ *Department of Physics & Meteorology,*

IIT Kharagpur, Kharagpur-721302, INDIA

² *Department of Physics, IIT Ropar, Rupnagar-140001, INDIA*

³ *Department of Physics, University of Lucknow, Lucknow-226007, INDIA and*

⁴ *Institute of Physics, Bhubaneswar-751005, INDIA*

Abstract

Spectroscopy of nuclei in the mass range $A = 76$ to $A = 130$, participating in double beta decay processes are studied in the framework of the self-consistent deformed Hartree-Fock (HF) and angular momentum (J) projection model. Spectra of ground bands have been studied and compared with available experimental results for even-even parent and daughter as well as for intermediate odd-odd nuclei. To test the reliability of the wave functions we have also calculated the reduced E2 transition matrix elements, electric quadrupole moments and magnetic dipole moments for these nuclei. The calculated results are compared with the experimental findings and substantial agreement is achieved.

PACS numbers: 21.10.-k, 21.60.-n, 23.20.-g, 27.60.+j

* email:surja@phy.iitkgp.ernet.in

I. INTRODUCTION

One of the most rarer processes of the nature, the double beta decay has unambiguous importance in explicitly linking nuclear structure aspects with neutrino physics [1–3]. Nuclear double beta decay is a second order process which involved electroweak decay of two nucleons simultaneously. The two neutrino mode of double beta decay is a second order process and allowed in standard model. It has been detected for nearly a dozen of nuclei [4]. The correct theoretical description of these observations serves as a test of various nuclear models and also a necessary step to understand the neutrinoless mode. The extraction of information is essentially dependent upon the prediction of Nuclear Transition Matrix Elements (NTMEs) involved in these processes. The difference in the configurations of the nucleons between initial and final states is a major ingredient of the matrix elements. The NTMEs contain the wave function of the initial even-even nucleus in its 0^+ ground state and the wave function of the final nucleus (usually 0^+ ground state but some time also excited 2^+ and 0^+ states). These wave functions are connected by proper operators. In case of two neutrino mode the summation over all 1^+ states of the intermediate odd-odd nuclei is required where as for neutrinoless decay the summation over the complete set of the states of intermediate nucleus is needed. Therefore it will be necessary to evaluate the structure of the initial, final and intermediate nuclei explicitly.

The most of the nuclei undergoing double beta decay are medium or heavy mass region and all of them are even even type, in which pairing degrees of freedom play an important role. Moreover it has been conjectured that the deformation plays a crucial role in double beta transitions. Hence it is desirable to have a model in which pairing and deformation degrees of freedom treated on equal footing in its formalism. The shell model, which attempts to solve the nuclear many-body problems as exactly as possible, is always being the best choice for model calculations. However, for most of the double beta decaying nuclei the full scale shell model calculations are not feasible and the reliability of theoretical predictions has been hampered by unstabilities in case of BCS+RPA type treatment. For this purpose the angular momentum projected deformed Hartree-Fock (DHF) model is one of the most convenient choices. The DHF formalism, the pairing interaction is taken into account by mixing particle-hole excitations (2p-2h,4p-4h etc) of $K = 0$ type across the Fermi surfaces over the HF ground state and deformation effects are included in a self-consistent way.

Moreover it has been shown [5] that it is possible to get shell model results with angular momentum projected DHF calculation by mixing only a few intrinsic configurations built by suitable particle-hole excitations across proton and neutron Fermi surfaces.

Here we have used microscopic many-body self consistent model based on deformed Hartree-Fock procedure and subsequent angular momentum projection technique for a reliable description of the nuclear structure of some medium as well heavy nuclei participating in double beta decay processes in the mass range $A = 76$ to 130. Since our aim is to study the low-lying spectroscopic properties of the nuclei, we have not incorporated the Coulomb effect in our calculations. The inclusion of Coulomb effect will not change the energy spectra and electromagnetic matrix elements of individual nucleus rather it will change the energy difference between two nuclei.

In the present article we briefly discuss about the theoretical formalism in Section 2. Section 3 contains the discussion about the results obtained from this paper. The conclusions are finally given in Section 4.

II. DEFORMED HARTREE-FOCK AND ANGULAR MOMENTUM (J) PROJECTION METHOD

In this section we present briefly the model used for the microscopic calculations. More details can be found in Refs. [6–9]. Our model consists of self-consistent deformed Hartree-Fock mean field obtained with a Surface Delta residual interaction and subsequent Angular momentum projection to obtain states with good angular momentum.

The axially deformed states $|\eta m\rangle$ are expanded in the spherical basis states as follows:

$$|\eta m\rangle = \sum_j C_{jm} |jm\rangle \quad (1)$$

where j is the angular momentum of the spherical single particle state and m its projection on symmetry axis. The mixing amplitude C_{jm} are obtained by solving deformed Hartree-Fock equations in an iterative process. When the convergence in the HF solutions is obtained we get deformed single particle orbits. The residual interaction is also included self-consistently and it causes the mixing of single-particle orbits of nucleons.

Because of mixing in single particle orbits, the HF configurations $|\phi_K\rangle$ are superposition of states of good angular momentum. The states of good angular momentum can be extracted

by means of projection operator [10]

$$P_K^{JM} = \frac{2J+1}{8\pi^2} \int d\Omega D_{MK}^J(\Omega)^* R(\Omega) \quad (2)$$

Here $R(\Omega)$ is the rotation operator $e^{-i\alpha J_z} e^{-i\beta J_y} e^{-i\gamma J_z}$ and Ω represents the Euler angles α , β and γ .

The Hamiltonian overlap between two states of angular momentum J projected from intrinsic states ϕ_{K_1} and ϕ_{K_2} is given by:

$$H_{K_1 K_2}^J = \frac{2J+1}{2} \frac{1}{(N_{K_1 K_1}^J N_{K_2 K_2}^J)^{1/2}} \int_0^\pi d\beta \sin(\beta) d_{K_1 K_2}^J(\beta) \times \langle \phi_{K_1} | H e^{-i\beta J_y} | \phi_{K_2} \rangle \quad (3)$$

with

$$N_{K_1 K_2}^J = \frac{2J+1}{2} \int_0^\pi d\beta \sin(\beta) d_{K_1 K_2}^J(\beta) \langle \phi_{K_1} | e^{-i\beta J_y} | \phi_{K_2} \rangle \quad (4)$$

Reduced matrix elements of tensor operator T^L between projected states $\psi_{K_1}^{J_1}$ and $\psi_{K_2}^{J_2}$ are given by

$$\langle \psi_{K_1}^{J_1} || T^L || \psi_{K_2}^{J_2} \rangle = \frac{1}{2} \frac{(2J_2+1)(2J_1+1)^{1/2}}{(N_{K_1 K_1}^{J_1} N_{K_2 K_2}^{J_2})^{1/2}} \sum_{\mu\nu} C_{\mu\nu K_1}^{J_2 L J_1} \times \int_0^\pi d\beta \sin(\beta) d_{\mu K_2}^{J_2}(\beta) \langle \phi_{K_1} | T_\nu^L e^{-i\beta J_y} | \phi_{K_2} \rangle \quad (5)$$

where the tensor operator T^L denotes electromagnetic operators of multipolarity L .

In general, two states $|\psi_{K_1}^{JM}\rangle$ and $|\psi_{K_2}^{JM}\rangle$ projected from two intrinsic configurations $|\phi_{K_1}\rangle$ and $|\phi_{K_2}\rangle$ are not orthogonal to each other even if the intrinsic states $|\phi_{K_1}\rangle$ and $|\phi_{K_2}\rangle$ are orthogonal. We orthonormalise them using following equation

$$\sum_{K'} (H_{KK'}^J - E_J N_{KK'}^J) b_{K'}^J = 0 \quad (6)$$

Here $N_{KK'}^J$ are amplitude overlap and $b_{K'}^J$ are the orthonormalised amplitudes, which can be identified as band-mixing amplitudes. The orthonormalised states are given by

$$\psi^{JM} = \sum_K b_K^J \psi_K^{JM} \quad (7)$$

With these orthonormalised states we can calculate matrix elements of various tensor operators.

The spectroscopic quadrupole moment of a state with angular momentum J is given by

$$Q_S(J) = \frac{1}{(2J+1)^{1/2}} \left(\frac{16\pi}{5} \right)^{1/2} C_{J0J}^{J2J} \langle \Psi_K^J || \sum_{i=p,n} Q_2^i || \Psi_K^J \rangle \quad (8)$$

where the summation is for quadrupole moment operators of protons and neutrons.

The gyromagnetic factor (g-factor) of state J is defined as

$$g(J) = \frac{\mu(J)}{J} \quad (9)$$

where $\mu(J)$ is the magnetic moment of state J. The magnetic dipole moment (μ) of a state with angular momentum J can be expressed as

$$\mu(J) = \frac{1}{(2J+1)^{1/2}} C_{J0J}^{J1J} \left(\sum_{i=p,n} \langle \Psi_K^J || g_l^i l_i + g_s^i s_i || \Psi_K^J \rangle \right) \quad (10)$$

where i=p and n for protons and neutrons respectively. where g_l and g_s are orbital and spin g-factor respectively. The g-factors of $g_l = 1.0\mu_N$ and $g_s = 5.586 \times 0.5\mu_N$ for protons and $g_l = 0\mu_N$ and $g_s = -3.826 \times 0.5\mu_N$ for neutrons are used for the calculations. The quenching of spin g-factors by 0.75 is taken in account to consider the core polarization effect [11, 12].

III. RESULTS AND DISCUSSION

The deformed HF orbits are calculated with a spherical core of ^{56}Ni , the model space spans the $1p_{3/2}$, $0f_{5/2}$, $1p_{1/2}$, $0g_{9/2}$, $0d_{5/2}$, $0g_{7/2}$, $0d_{3/2}$, $2s_{1/2}$ and $0h_{11/2}$ orbits both for protons neutrons with single particle energies 0.0, 0.78, 1.88, 4.44, 8.88, 11.47, 10.73, 12.21 and 13.69 MeV respectively. We use a surface delta interaction [13] (with interaction strength ~ 0.36 for $p-p$, $p-n$ and $n-n$ interactions) as the residual interaction among the active nucleons in these orbits.

Deformed Hartree-Fock and Angular Momentum Projection calculations are performed for some medium-heavy nuclei with mass number $A = 76$ to $A = 130$. In our model we can calculate the energy spectra and other electromagnetic moments for even-even parents and daughter as well as odd-odd intermediate nuclei. This is an interesting feature of our model.

In contrast to PSM where a large number of configurations is needed to understand low-lying yrast spectra, it is found that angular momentum projection (AMP) from a few low-lying configurations can reasonably reproduces the yrast-spectra. Sometimes the AMP from single K configuration gives fairly good description of yrast structure. This is due

to fact that the residual interaction is included self-consistently in the HF calculations, so that the HF configurations and various particle-hole configurations built on HF solutions are already closer to the solutions obtained from full many body Schrödinger equations.

The Hartree-Fock solutions for the parent, intermediate and daughter nuclei are given in Table I. The values of intrinsic quadrupole moments(Q_{20}) are given both for proton and neutron in unit of harmonic oscillator length parameter, b ($= 0.9A^{1/3} + 0.7\text{fm}$).

TABLE I: Hatree-Fock Solution of the Nuclei

Nucleus	Shape	E_{HF} (in MeV)	$\langle Q_{20} \rangle$ (in b^2)	
			Proton	Neutron
^{76}Ge	Prolate	-45.772	3.964	4.659
	Oblate	-43.672	-2.995	-3.439
^{76}As	Prolate	-48.909	4.181	6.712
	Oblate	-46.819	-3.675	-2.952
^{76}Se	Prolate	-55.613	4.699	8.894
	Oblate	-54.573	-4.582	-2.518
^{78}Kr	Prolate	-72.058	8.573	10.372
	Oblate	-71.054	-7.274	-6.739
^{78}Br	Prolate	-68.389	8.259	9.599
	Oblate	-67.104	-4.634	-2.978
^{78}Se	Prolate	-59.584	4.711	7.640
	Oblate	-57.790	-4.565	-3.452
^{82}Se	Prolate	-64.588	4.648	4.865
	Oblate	-61.932	-4.626	-4.020
^{82}Br	Prolate	-68.428	3.821	5.129
	Oblate	-66.674	-4.297	-3.794
^{82}Kr	Prolate	-77.646	3.210	4.789
	Oblate	-77.107	-3.767	-3.330
^{96}Mo	Prolate	-91.214	3.745	5.820
	Oblate	-90.418	-2.518	-3.445

Continued on next page...

TABLE I – Continued

Nucleus	Shape	E_{HF} (in MeV)	$\langle Q_{20} \rangle$ (in b^2)	
			Proton	Neutron
^{96}Tc	Prolate	-98.572	4.562	5.456
	Oblate	-96.403	-2.976	-3.361
^{96}Ru	Prolate	-106.457	5.951	6.037
	Oblate	-103.387	-3.406	-3.795
^{100}Mo	Prolate	-107.174	3.694	5.390
	Oblate	-105.160	-2.515	-1.677
^{100}Tc	Prolate	-118.232	9.857	10.681
	Oblate	-112.926	-3.004	-3.016
^{100}Ru	Prolate	-127.008	6.338	8.198
	Oblate	-123.029	-3.386	-3.399
^{106}Cd	Prolate	-172.047	6.079	10.236
	Oblate	-167.235	-9.462	-11.471
^{106}Ag	Prolate	-166.746	6.581	9.761
	Oblate	-164.073	-8.909	-10.966
^{106}Pd	Prolate	-159.401	6.916	8.847
	Oblate	-156.593	-6.728	-9.381
^{110}Pd	Prolate	-170.686	6.079	6.754
	Oblate	-170.009	-4.862	-7.360
^{110}Ag	Prolate	-183.424	5.474	7.796
	Oblate	-181.197	-11.114	-15.346
^{110}Cd	Prolate	-196.677	5.621	9.471
	Oblate	-192.382	-12.079	-14.254
^{116}Cd	Prolate	-202.919	6.337	10.633
	Oblate	-200.953	-2.575	-4.562
^{116}In	Prolate	-211.305	10.883	13.402
	Oblate	-210.156	-11.879	-15.857

Continued on next page...

TABLE I – Continued

Nucleus	Shape	E_{HF} (in MeV)	$\langle Q_{20} \rangle$ (in b^2)	
			Proton	Neutron
^{116}Sn	Prolate	-220.357	1.969	4.177
	Oblate	-219.197	-1.183	-5.466
^{124}Sn	Prolate	-229.001	2.899	3.670
	Oblate	-228.494	-2.147	-4.587
^{124}Sb	Prolate	-237.729	2.575	2.839
	Oblate	-240.753	-5.044	-9.165
^{124}Te	Prolate	-246.776	3.652	2.008
	Oblate	-250.869	-5.649	-9.108
^{130}Te	Prolate	-267.880	4.737	4.587
	Oblate	-268.664	-3.716	-3.670
^{130}I	Prolate	-273.928	4.806	4.616
	Oblate	-274.691	-3.896	-7.477
^{130}Xe	Prolate	-291.346	5.105	7.570
	Oblate	-291.945	-3.891	-8.331

A. Energy Spectra

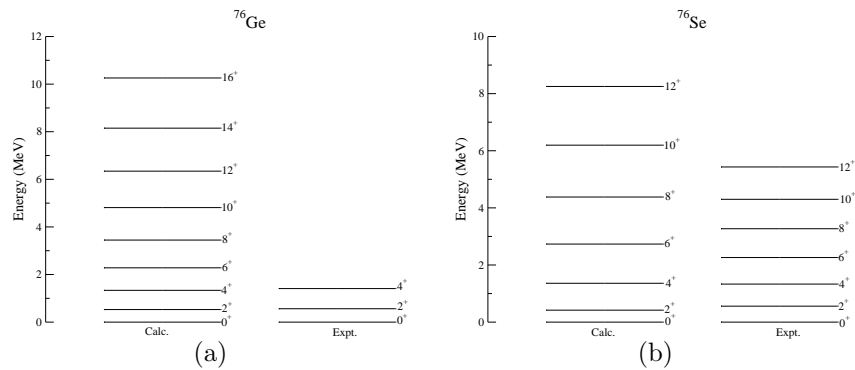


FIG. 1: Energy spectra for ^{76}Ge and ^{76}Se nuclei. The experimental values are taken from Ref. [14]

In Fig. 1 we have shown the low-lying spectra for the nuclei participating in the double beta decay processes of ^{76}Ge . In case of the odd-odd intermediate nucleus ^{76}As , the experimental energy spectra is not known therefore we are also not showing the theoretical spectra for these nuclei. For the nuclei ^{76}Ge and ^{76}Se we have considered the prolate solutions as the prolate solutions are energetically lower than oblate solutions. The angular momentum projected results in comparison with the available experimental data are shown in Figure 1.

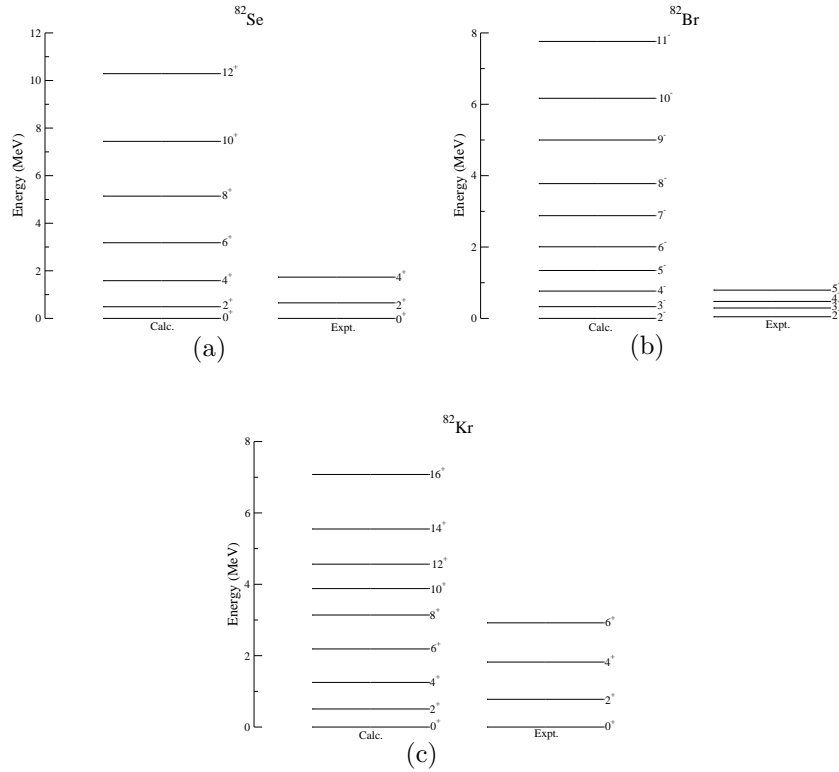


FIG. 2: Energy spectra for ^{82}Se , ^{82}Br and ^{82}Kr nuclei. The experimental values are taken from Ref. [15]

The energy spectra of ^{82}Se , ^{82}Br and ^{82}Kr are shown in Fig. 2. The angular momentum projection results considering the prolate solutions of ^{82}Se and ^{82}Br are shown in Fig. 2(a) and Fig. 2(b). In case of ^{82}Kr , the prolate and oblate solutions are degenerate. So for this nucleus we have performed the shape-mixing calculation by mixing the prolate and oblate configurations. The shape-mixing calculation reasonably reproduces the low lying spectra for ^{82}Kr as can be seen in Fig. 2(c).

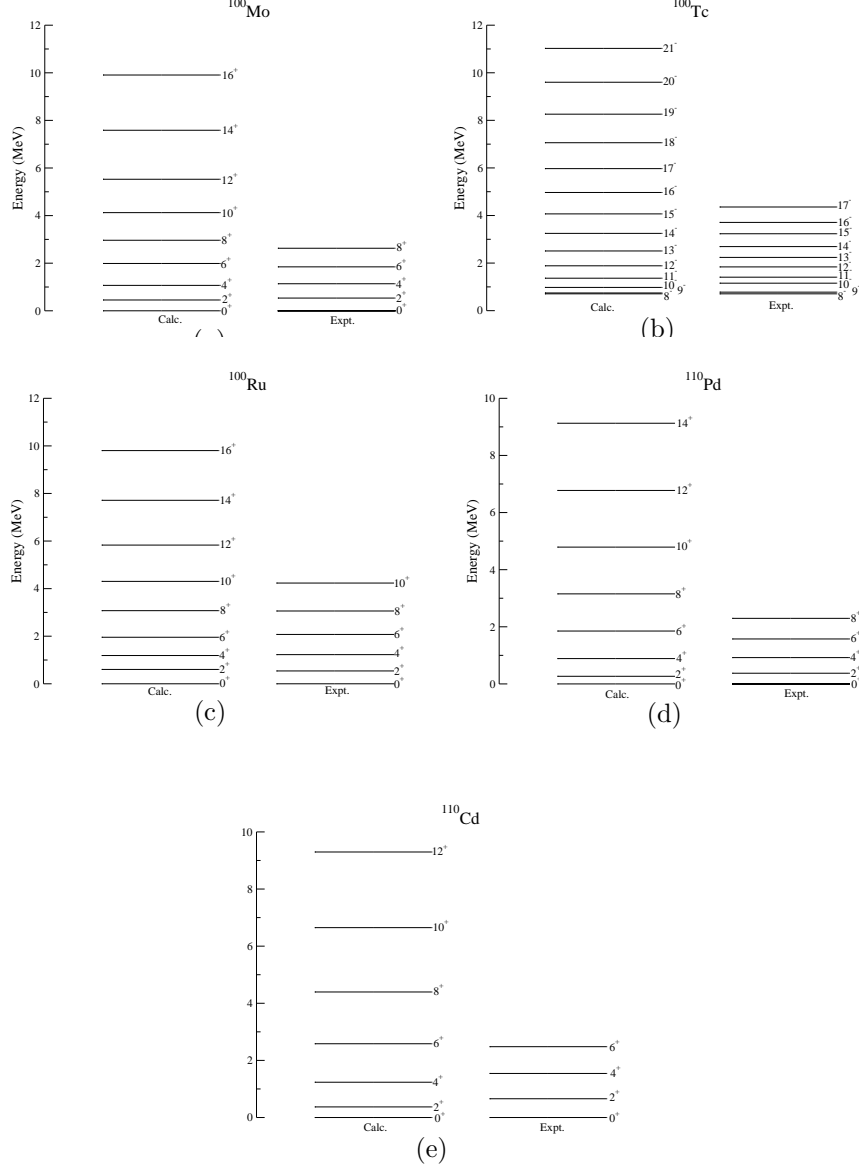


FIG. 3: Energy spectra for ^{100}Mo , ^{100}Tc , ^{100}Ru , ^{110}Pd and ^{110}Cd nuclei. The experimental values are taken from Refs. [16, 17]

The comparison of calculated and experimental results for nuclei ^{100}Mo , ^{100}Tc , ^{100}Ru , ^{110}Pd and ^{110}Cd are shown in Fig. 3. A fairly good agreement between theoretical and experimental spectra is obtained for them.

The nucleus ^{116}Cd exhibits a complex structure as it has active protons near $Z = 50$ shell closure and active neutrons near the neutron midshell. Our self-consistent calculations reproduce the band structure quit well. The compression in the ground band near $J = 8\hbar$ is

occurring due to the crossing of 2-proton excitation bands across $Z = 50$ shell. Apart from the ground band we have calculated two excited $K = 0^+$ bands compared with experimental results in Fig. 4(a). Similarly we have calculated the ground band for the daughter nucleus ^{116}Sn and shown in Fig. 4(b).

In Fig. 5(a) we have plotted the ground state spectra for ^{124}Sn . The Te isotopes are 2 protons above the tin shell closure. The ground band spectra for ^{124}Te are shown in Figs. 5(b). In Fig. 6(a), the energy spectra of ^{130}Te are given. We have used the oblate solutions for $^{128,130}\text{Te}$ as they are lower in energy in these two nuclei. The ^{130}Xe isotope shows interesting feature. The interplay between prolate and oblate shapes are observed in our calculations. The band spectra for ^{130}Xe are shown in Fig 6(b). The low spin states of this isotope are of prolate shape but for the states above $J = 6\hbar$ the calculations with oblate shapes are more closer to the experimental levels.

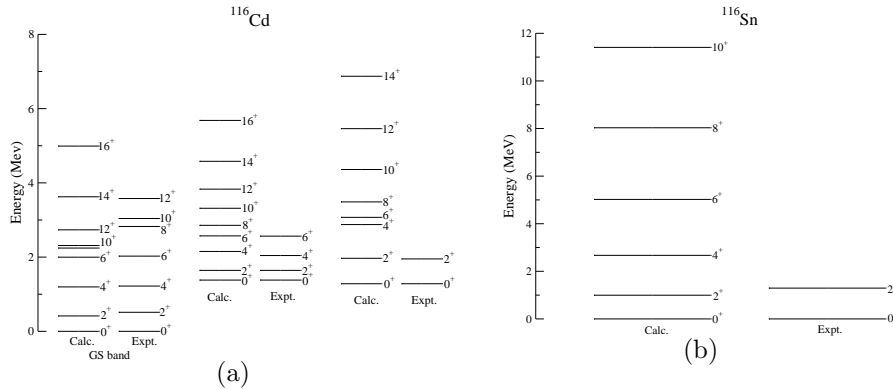


FIG. 4: Energy spectra for ^{116}Cd and ^{116}Sn nuclei. The experimental values are taken from Refs. [18]

The nuclei ^{78}Kr , ^{96}Ru and ^{106}Cd are the most promising nuclei among six which can decay through all three possible channels of positron double beta decay. In our present study we have considered these double beta decay nuclei to study the low-lying spectroscopy properties.

For ^{78}Kr , the energy spectra are shown in Fig. 7(a). Apart from the ground band we have shown the excited $K = 2^+$ band. The signature effect is observed in this band due

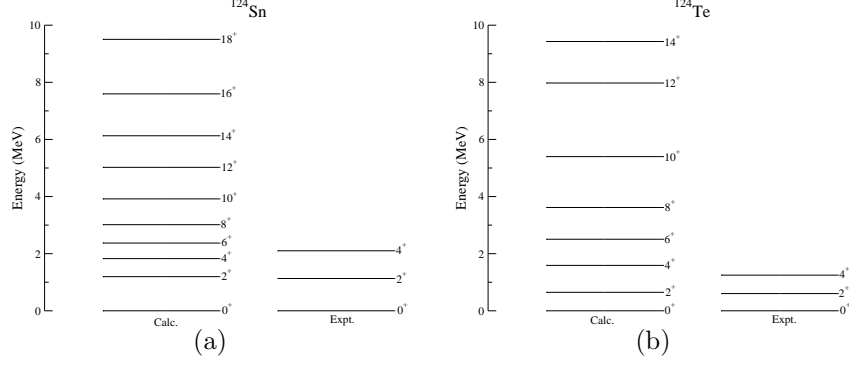


FIG. 5: Energy spectra for ^{124}Sn and ^{124}Te nuclei. The experimental values are taken from Refs. [19]

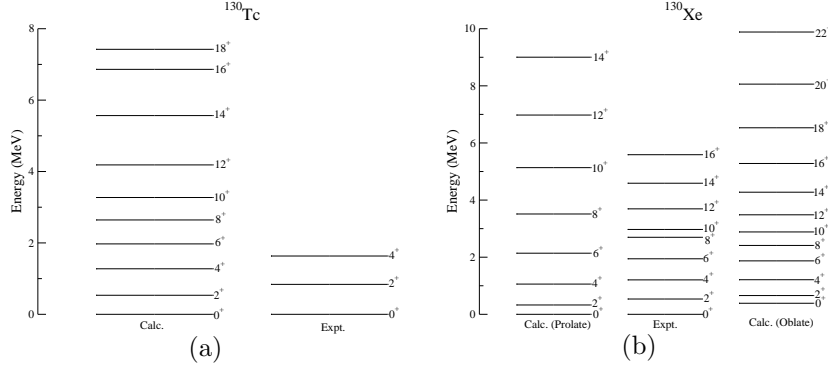


FIG. 6: Energy spectra for ^{130}Te and ^{130}Xe nuclei. The experimental values are taken from Refs. [20]

to the rotational alignment of $\nu g_{9/2}$. Similarly for ^{78}Se nucleus, the ground and excited $K = 2^+$ bands are shown in Fig. 7(b). For the $K = 2^+$ band the signature inversion is observed as a result of band crossing between $\nu f_{5/2} \nu g_{9/2}$ decoupled band with $K = 2^+$ and $K = 1^+$. In these nuclei the rotational behaviour of the ground band reproduces quite well except the $2^+ \rightarrow 0^+$ separation. This is probably due to the fact that in our formalism the pairing is not included explicitly which may be important in these nuclei.

In Figs. 8 and 9 we have shown the calculated ground band in comparison with experimentally available results for the nuclei ^{96}Ru , ^{96}Mo , ^{106}Cd , ^{106}Ag and ^{106}Pd . Our theoretically calculated results are in reasonably good agreement with the experimentally known values.

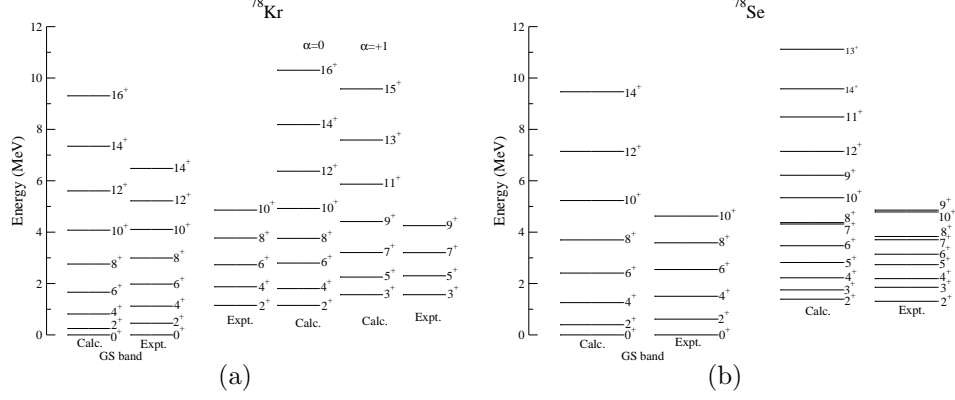


FIG. 7: Energy spectra for ^{78}Kr and ^{78}Se nuclei The experimental values are taken from Refs. [21]

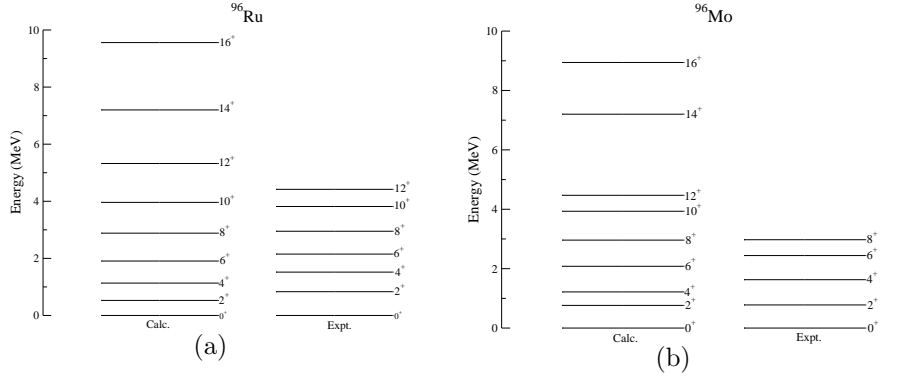


FIG. 8: Energy spectra for ^{96}Ru and ^{96}Mo nuclei The experimental values are taken from Refs. [22]

B. Electromagnetic Properties

We have calculated the reduced transition moments, quadrupole moments and magnetic dipole moments. These values are presented in Tables II and III.

In Table II we have shown the calculated $B(E2; 0^+ \rightarrow 2^+)$ for the ground band of the even-even parent and daughter nuclei. The values are calculated for the effective charges $e_p = 1 + e_{ff}$ and $e_n = e_{ff}$ for protons and neutrons respectively where e_{ff} varies for three different values 0.4, 0.5 and 0.6. Comparison between theoretical and experimental values are also made in this table and we obtained a reasonable agreement for all the nuclei studied here except for ^{116}Cd , ^{116}Sn and ^{124}Te . But still our calculated results are much better reproduced than the values predicted by some other models e. g. WoodsSaxon model and HartreeFock + BCS calculations with the Skyrme SIII force (see Ref. [24] for the values calculated with these model) for these isotopes. The nuclei upto $A = 82$, the values are

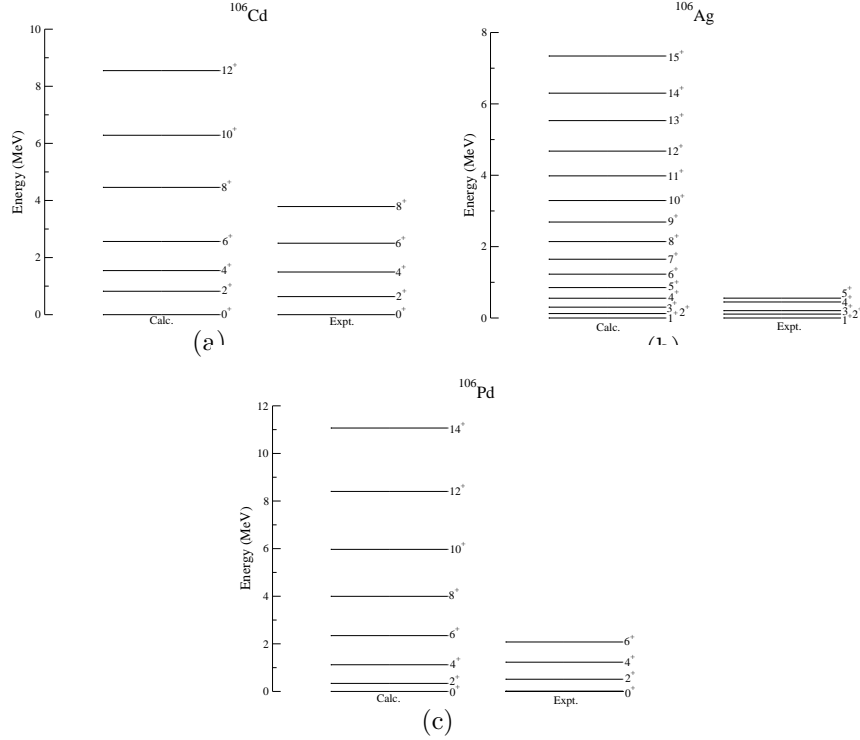


FIG. 9: Energy spectra for ^{106}Cd , ^{106}Ag and ^{106}Pd nucleus. The experimental values are taken from Ref. [23]

better reproduced by taking $e_{ff} = 0.5$ where as for the nuclei above this mass range the values those are calculated with $e_{ff} = 0.6$ are more close to the experimental results.

The calculated quadrupole moments are given in columns 3-5 of Table III. The values are calculated with the same effective charges as in case of B(E2). Experimental values are not available for ^{78}Kr , ^{78}Br , ^{82}Kr , ^{96}Tc , ^{100}Tc , ^{106}Ag , ^{130}I and ^{130}Xe . In the last two columns of Table III presents the theoretically calculated and experimental results for magnetic dipole moments respectively. The spin and parity of the corresponding states are given in Table III. Our calculations correctly reproduce the sign and the values are reasonably agree with that of experimentally observed for most of the nuclei. For ^{82}Kr and ^{106}Pd the calculated values are different from experimental data by 0.6 and 0.8 respectively.

TABLE II: Comparison of calculated and experimentally observed reduced transition probabilities $B(E2:0^+ \rightarrow 2^+)$. Here $B(E2)$ are calculated for effective charge $e_p = 1 + e_{eff}$ and $e_n = e_{eff}$. In the last column the values marked by * are average $B(E2)$ values from Ref. [24]

Parent	$B(E2:0^+ \rightarrow 2^+) (e^2b^2)$				Daughter	$B(E2:0^+ \rightarrow 2^+) (e^2b^2)$			
Nucleus	Theory			Experiment[24]	Nucleus	Theory			Experiment[24]
	e_{eff}					e_{eff}			
	0.40	0.50	0.60			0.40	0.50	0.60	
^{76}Ge	0.195	0.242	0.295	0.268±0.008*	^{76}Se	0.311	0.400	0.501	0.420±0.010*
				0.230±0.035					0.39±0.26
				0.290±0.030					0.43±0.06
^{78}Kr	0.521	0.650	0.793	0.633±0.039*	^{78}Se	0.200	0.254	0.314	0.335±0.009*
				0.54±0.13					0.327±0.007
				0.686±0.030					0.40±0.07
^{82}Se	0.161	0.197	0.237	0.185±0.002*	^{82}Kr	0.155	0.192	0.232	0.223±0.010*
				0.213±0.019					0.19±0.05
				0.179±0.019					0.225±0.009
^{96}Mo	0.138	0.175	0.216	0.271±0.005*	^{96}Ru	0.143	0.176	0.212	0.251±0.010*
				0.310±0.047					0.268±0.032
				0.302±0.039					0.236±0.007
^{100}Mo	0.306	0.394	0.493	0.516±0.010*	^{100}Ru	0.306	0.390	0.484	0.490±0.005*
				0.511±0.009					0.493±0.003
				0.526±0.026					0.494±0.006
^{106}Cd	0.464	0.598	0.749	0.410±0.020*	^{106}Pd	0.439	0.552	0.679	0.660±0.035*
				0.47±0.05					0.689±0.37
				0.384±0.005					0.59±0.009
^{110}Pd	0.498	0.617	0.750	0.870±0.040*	^{110}Cd	0.484	0.617	0.767	0.450±0.020*

Continued on next page...

TABLE II – Continued

Parent	$B(E2:0^+ \rightarrow 2^+) (e^2b^2)$			Daughter	$B(E2:0^+ \rightarrow 2^+) (e^2b^2)$				
Nucleus	Theory			Nucleus	Theory				
	e_{eff}				e_{eff}				
	0.40	0.50	0.60		0.40	0.50	0.60		
							0.78±0.12	0.504±0.040	
							0.820±0.080	0.447±0.035	
¹¹⁶ Cd	0.197	0.237	0.281	0.560±0.020*	¹¹⁶ Sn	0.064	0.084	0.106	0.209±0.006*
									0.501±0.047
									0.183±0.037
									0.608±0.030
									0.165±0.030
¹²⁴ Sn	0.0875	0.102	0.125	0.1160±0.0040*	¹²⁴ Te	0.107	0.132	0.160	0.568±0.006*
									0.140±0.030
									0.39±0.08
									0.188±0.013
									0.539±0.028
¹³⁰ Te	0.149	0.189	0.229	0.295±0.007*	¹³⁰ Xe	0.297	0.377	0.465	0.65±0.05*
									0.290±0.011
									0.631±0.048
									0.260±0.050
									0.640±0.160

TABLE III: Comparison of calculated and experimentally observed static quadrupole moments $Q(J^\pi)$ and magnetic dipole moments $\mu(J^\pi)$. Here $Q(J^\pi)$ are calculated for effective charge $e_p = 1 + e_{eff}$ and $e_n = e_{eff}$.

Nucleus	J^π	$Q(J^\pi)$ (eb)			$\mu(J^\pi)$ (nm)		
		Theory	Experiment[25]		Theory	Experiment[25]	
		e_{eff}					
		0.40	0.50	0.60			
⁷⁶ Ge	2 ⁺	-0.166	-0.167	-0.168	-0.19±0.06	0.582	0.84±0.05
							0.67±0.08

Continued on next page...

TABLE III – Continued

Nucleus	J^π	$Q(J^\pi)$ (eb)				$\mu(J^\pi)$ (nm)	
		Theory			Experiment[25]	Theory	Experiment[25]
		e_{eff}					
		0.40	0.50	0.60			
							0.56±0.12
⁷⁶ As	2 ⁻	0.249	0.278	0.307	7±8	-0.775	-0.906±0.005
							(-)0.9028±0.0010
⁷⁶ Se	2 ⁺	-0.423	-0.479	-0.563	-0.34±0.07	0.637	0.81±0.05
							+0.8±0.2
⁷⁸ Kr	2 ⁺	-0.654	-0.730	-0.806		0.998	+0.86±0.02
							+1.08±0.10
⁷⁸ Br	1 ⁺	0.217	0.243	0.268		0.255	0.13±0.03
⁷⁸ Se	2 ⁺	-0.405	-0.456	-0.508	-0.26±0.09	0.541	0.77±0.05
							+0.8±0.2
⁸² Se	2 ⁺	-0.365	-0.405	-0.444	-0.22±0.07	0.937	0.99±0.06
							0.9±0.3
⁸² Br	5 ⁻	0.659	0.735	0.812	0.69±0.02	1.216	+1.6270±0.0005
					0.748±0.10		
⁸² Kr	2 ⁺	-0.706	-0.796	-0.866		0.202	0.80±0.03
⁹⁶ Mo	2 ⁺	-0.334	-0.376	-0.418	-0.20±0.08	+0.91	+0.79±0.06
					or +0.04±0.08		
⁹⁶ Tc	7 ⁺	0.534	0.605	0.676	-	4.618	5.09±0.05
							+5.04±0.08
⁹⁶ Ru	2 ⁺	-0.338	-0.375	-0.412	-0.13±0.09	1.482	-
					-0.1±0.2		
					-0.2±0.3		
¹⁰⁰ Mo	2 ⁺	-0.598	-0.665	-0.738	-0.42±0.09	+1.05	+0.94±0.07
					-0.39±0.08		+0.7±0.4

Continued on next page...

TABLE III – Continued

Nucleus	J^π	$Q(J^\pi)$ (eb)				$\mu(J^\pi)$ (nm)	
		Theory			Experiment[25]	Theory	Experiment[25]
		e_{eff}					
		0.40	0.50	0.60			
^{100}Tc	1^+	0.214	0.237	0.260	-	-1.688	-
^{100}Ru	2^+	-0.486	-0.55	-0.614	-0.54 ± 0.07	0.98	$+1.02\pm 0.13$
					-0.40 ± 0.12		
					-0.43 ± 0.07		
^{106}Cd	2^+	-0.575	-0.584	-0.654	-0.28 ± 0.08	0.749	$+0.8\pm 0.2$
^{106}Ag	1^+	0.189	0.213	0.238	-	+2.348	$+2.9\pm 0.2$
^{106}Pd	2^+	-0.599	-0.672	-0.745	-0.56 ± 0.08	0.711	$+0.80\pm 0.04$
					-0.51 ± 0.07		
^{110}Pd	2^+	-0.536	-0.597	-0.658	-0.62 ± 0.06	1.122	-0.47 ± 0.03
					-0.70 ± 0.06		-0.55 ± 0.08
					0.74 ± 0.06		
^{110}Ag	1^+	0.193	0.219	0.244	0.24 ± 0.12	2.715	2.7271 ± 0.0008
^{110}Cd	2^+	-0.515	-0.549	-0.654	-0.40 ± 0.04	0.637	$+0.57\pm 0.11$
					-0.39 ± 0.05		$+0.56\pm 0.10$
					-0.36 ± 0.08		0.62 ± 0.14
^{116}Cd	2^+	-0.334	-0.365	-0.396	-0.42 ± 0.04	+1.416	$+0.60\pm 0.14$
					-0.42 ± 0.08		
					-0.64 ± 0.12		
^{116}In	1^+	0.300	0.335	0.370	0.11 ± 0.01	2.7645	2.7876
^{116}Sn	2^+	-0.203	-0.230	-0.258	-0.17 ± 0.04	0.358	-0.3 ± 0.2
^{124}Sn	2^+	-0.246	-0.276	-0.305	0.0 ± 0.2	-0.246	-0.3 ± 0.2
^{124}Sb	3^-	0.580	0.653	0.725	1.20 ± 0.02	1.624	$+1.9\pm 0.4$
^{124}Te	2^+	0.286	0.318	0.350	-0.45 ± 0.05	0.649	$+0.56\pm 0.06$
							$+0.66\pm 0.06$

Continued on next page...

TABLE III – Continued

Nucleus	J^π	$Q(J^\pi)$ (eb)				$\mu(J^\pi)$ (nm)	
		Theory		Experiment[25]	Theory	Experiment[25]	
		e_{eff}					
		0.40	0.50	0.60			
						+0.62±0.08	
^{130}Te	2^+	-0.345	-0.386	-0.428	-0.15±0.10	0.420	+0.58±0.10
							+0.66±0.16
^{130}I	5^+	0.967	1.085	1.202	-	3.708	3.349±0.007
^{130}Xe	2^+	-0.491	-0.552	-0.614	-	0.611	+0.67±0.02
							+0.76±0.14
							+0.62±0.08

IV. CONCLUSION

To summarize, we have quantified the calculated deformed Hartree-Fock wave functions by comparing the calculated values with experimental data for a number of nuclear properties like band spectra, reduced E2 transition matrix elements, quadrupole moments and magnetic dipole moments of nuclei involved in double beta decay processes. A reasonable agreement between calculated and experimentally observed quantities make us confident about the reliability of the deformed few body wave functions obtained in our microscopic self-consistent calculations. These wave functions will further be employed for nuclear transition matrix elements calculations of double beta decay transitions.

Acknowledgments

CRP acknowledges the support of the Department of Science and Technology, India (DST Project SR/S2/HEP-37/2008) during this work.

- [1] F. Bohm and P. Vogel, *Physics of Massive Neutrinos*, Cambridge University Press, 2nd edition, Cambridge, (1992).
- [2] W. C. Haxton and G. J. Stephenson Jr., *Prog. Part. Nucl. Phys.*, **12**, 409 (1984).
- [3] M. Moe and P. Vogel, *Ann. Rev. of Nucl. Part. Sci.*, **44**, 247 (1994).
- [4] J. D. Vergados, *Phys. Rep.*, **361**, 1 (2002).
- [5] S. B. Khadkikar, S. C. K. Nair and S. P. Pandya, *Phys. Lett.* **B36** 290 (1971).
- [6] G. Ripka, *Advances in Nuclear Physics*, **Vol. 1** (1966) Ed. M. Baranger and E. Vogt (Plenum).
- [7] C.R. Praharaaj, in *Structure Of Atomic Nuclei*, Ed. L. Satpathy (Narosa Publication House, New Delhi), p-108 (1999).
- [8] C.R. Praharaaj, *J. Physics* **G14** (1988)843; *Phy. Lett.* **B119** 17(1982).
- [9] S. K. Ghorui *et al.*, arXiv:nucl-th/1106.3152v1 (submitted to *Phys. Rev. C*)
- [10] R.E. Peierls, Y. Yoccoz, *Proc. Phys. Soc.* **A70**, 381 (1957).
- [11] S. G. Nilsson and O. Prior, *Mat. Fys. Medd. Da. Vid. Selsk.*, **29**, no. 16 (1961).
- [12] Z. Bochnacki and S. Ogaza, *Nucl. Phys.* **69**, 186 (1965).
- [13] A. Faessler, P. Plastino and S.A. Moszkowski, *Phys. Rev.* **156**, 1064 (1967).
- [14] B. Singh, D.A. Viggars, *Nucl. Data Sheets* **42**, 233-368 (1984).
- [15] J. K. Tuli, *Nucl. Data Sheets* **98**, 209-334 (2003).
- [16] Balraj Singh, *Nucl. Data Sheets* **81**, 1-182 (1997).
- [17] D. De Frenne, E. Jacobs, *Nucl. Data Sheets* **89**, 481-640 (2000).
- [18] Jean Blachot, *Nucl. Data Sheets* **92**, 455-622 (2001).
- [19] J. Katakura, Z.D. Wu, *Nucl. Data Sheets* **109**, 1655-1877 (2008).
- [20] Balraj Singh, *Nucl. Data Sheets* **93**, 33-242 (2001).
- [21] AMEENAH R. FARHAN and BALRAJ SINGH, *Nucl. Data Sheets* **110**, 19172080 (2009).
- [22] D. Abriola, A.A. Sonzogni, *Nucl. Data Sheets* **109**, 2501-2655 (2008).
- [23] D. De Frenne, A. Negret, *Nucl. Data Sheets* **109**, 943-1102 (2008).

- [24] S. Raman *et al.*, *At. Data Nucl. Data Tables* **78**, 1 (2001).
- [25] N. J. Stone, *At. Data Nucl. Data Tables* **90**, 75 (2005).